

Highlights

GLAI: GreenLightningAI for Accelerated Training through Knowledge Decoupling

Jose I. Mestre, Alberto Fernández-Hernández, Cristian Pérez-Corral, Manuel F. Dolz, Jose Duato, Enrique S. Quintana-Ortí

- Introduces GLAI for fast retraining by decoupling routing and weight updates.
- Models ReLU MLPs using paths of active neurons with fixed activation decisions.
- Retrains only the path weights, avoiding full weight re-optimization.
- Uses a compact estimator to select active neuron paths during retraining.
- Enables efficient fine-tuning as a drop-in replacement in common workflows.

GLAI: GreenLightningAI for Accelerated Training through Knowledge Decoupling

Jose I. Mestre^a, Alberto Fernández-Hernández^a, Cristian Pérez-Corral^a,
Manuel F. Dolz^b, Jose Duato^c, Enrique S. Quintana-Ortí^a

^a*Universitat Politècnica de València, Valencia, Spain*

^b*Universitat Jaume I, Castellón de la Plana, Spain*

^c*Openchip & Software Technologies, Barcelona, Spain*

Abstract

In this work we introduce GreenLightningAI (GLAI), a new architectural block designed as an alternative to conventional Multilayer Perceptrons (MLPs). The central idea is to separate two types of knowledge that are usually entangled during training: (i) *structural knowledge*, encoded by the stable activation patterns induced by Rectified Linear Unit (ReLU) activations; and (ii) *quantitative knowledge*, carried by the numerical weights and biases. By fixing the structure once stabilized, GLAI reformulates the MLP as a combination of paths, where only the quantitative component is optimized. This reformulation preserves the universal approximation capabilities of MLPs, while providing statistically significant evidence of faster training than the MLPs it replaces, with an average wall-clock speedup of $1.92\times$ across the six experimental settings. Crucially, GLAI is not just another classifier, but a generic block with the potential to replace MLPs for some tasks, from supervised heads with frozen backbones to projection layers in self-supervised learning or few-shot classifiers. Across diverse experimental setups, GLAI consistently matches or exceeds the accuracy of MLPs with an equivalent number of parameters, while reducing training time on average. Overall, GLAI establishes a new design principle that opens a direction for future

Email addresses: jimesmir@disca.upv.es (Jose I. Mestre), a.fernandez@upv.es (Alberto Fernández-Hernández), cperc@upv.es (Cristian Pérez-Corral), dolzm@uji.es (Manuel F. Dolz), jose.duato@openchip.com (Jose Duato), quintana@disca.upv.es (Enrique S. Quintana-Ortí)

All authors contributed equally to this work.

integration into large-scale architectures such as Transformers, where MLP blocks dominate the computational footprint.

Keywords: GreenLightningAI (GLAI), Knowledge Decoupling, Efficient Retraining, Fine-tuning, Multilayer Perceptrons, ReLU Networks, Activation pattern, Path Selector and Estimator

1. Introduction

Multilayer Perceptrons (MLPs) have consistently remained at the core of modern Deep Learning (DL) architectures. From the early theoretical foundations in the late 20th century [1, 2, 3], to the emergence of recurrent networks and the introduction of LSTMs for sequence modeling [4], the breakthrough of convolutional networks for computer vision [5, 6], the dominance of Transformers across modalities [7, 8, 9, 10], and the recent rise of sparsely-gated Mixture-of-Experts (MoE) architectures [11], MLPs have persisted as a fundamental building block. This endurance is explained by its strong expressive capacity: MLPs are universal approximators of nonlinear functions, capable of representing arbitrarily complex mappings. A central aspect of this expressivity arises from the combinatorial structure induced by activation functions such as Rectified Linear Unit (ReLU), which partition the input space into a collection of regions, each one defining a linear relationship between inputs and outputs, determined by binary activation patterns [12, 13].

Despite their central role, the training of MLP modules remains both costly and opaque. To clarify this process, a conceptual distinction between two forms of knowledge can be established. We revisit this distinction here and develop it mathematically, using it as the foundation on which the posterior framework is built. The first is *structural knowledge*, referring to the discrete activation patterns that determine how information flows through the network. The second is *quantitative knowledge*, which refers to the numerical values generated by each neuron and subsequently propagated and combined. The same study further showed that structural knowledge converges much earlier than its quantitative counterpart: activation patterns stabilize after relatively few training epochs, whereas the numerical outputs continue to evolve as the weights adjust over longer timescales. This observation motivates the possibility of decoupling the two components, freezing the structural part once it has converged, and retraining only the quantitative one.

Building directly on this theoretical result, we present GreenLightningAI (GLAI), the first architecture to operationalize this principle. GLAI is designed as a drop-in replacement for an MLP: it preserves equivalent representational power while enabling substantially faster training. The core idea is simple: a reduced-size MLP is trained until structural knowledge has converged; its activation patterns are then frozen, transforming the network into a fixed piecewise-linear system. At this point, the model can be re-expressed as a linear operator over all active paths, which can be efficiently re-trained. By fixing a sufficiently mature structural representation, GLAI guarantees expressivity while dramatically accelerating the quantitative optimization.

Our contributions can be summarized as follows:

1. We introduce GLAI, an architectural paradigm that replaces conventional ReLU-based MLPs with an equivalent formulation of comparable parameter count. We provide formal foundations, including proofs that any MLP can be re-expressed as a GLAI model without loss of expressive power.
2. We empirically show that decoupling structural from quantitative knowledge allows GLAI to optimize more efficiently, converging in fewer update steps while matching or even surpassing the accuracy of standard MLPs.
3. We validate the generality of GLAI in settings where MLPs play a central role: supervised heads on frozen backbones for classification, projection layers in self-supervised learning, and few-shot adaptation. These scenarios demonstrate both scalability across model widths and depths, and practical utility in domains such as computer vision and language processing.

This work positions GLAI as a new design principle for feedforward components, rather than as a task-specific model. While our present focus is on replacing isolated MLPs, the formulation may provide a basis for future exploration in larger architectures such as Transformers, where stacked MLPs account for a substantial share of computation. Assessing how GLAI can be effectively integrated into such settings remains an open direction for further research.

The remainder of the paper is organized as follows. Section 2 reviews related work in the areas of network structure, interpretability, and training

acceleration. Section 3 introduces the theoretical foundations of our approach, including formal definitions and the mathematical structure of the GLAI framework. Section 4 presents the experimental evaluation across diverse use cases and configurations. Finally, Section 5 concludes the paper and discusses future research directions.

2. Related Work

The foundations of GLAI build upon prior work by [14], which introduced the formal separation of structural and quantitative knowledge in ReLU-based Deep Neural Networks (DNNs) and demonstrated that activation patterns stabilize well before the numerical parameters converge. Some references regarding the study of metrics designed to assess changes in activation patterns include the works by [15] and [16], which evaluate the variability of structural knowledge and provide further evidence of its convergence during training.

This perspective connects naturally with earlier analyses of ReLU-based MLPs as piecewise linear functions. Work by [12] demonstrated the exponential growth of linear regions with depth, while [17] showed that practical MLPs typically operate in far fewer regions. Such results suggest that the effective complexity of a trained MLP is lower than its theoretical capacity. GLAI leverages this observation by intervening once the MLP head has implicitly committed to a stable subset of linear regions sufficient for the task.

Several authors have further developed path- and region-based views of ReLU-based MLPs. For instance, [18] proposed the \mathcal{G} -space framework, optimizing directly over active paths, while [19] introduced Aletheia to interpret networks by decomposing them into local linear models. These works highlight the explanatory and computational value of activation patterns and paths. GLAI builds on similar conceptual foundations but shifts the emphasis: instead of optimizing in a transformed parameter space or prioritizing interpretability, our approach treats paths as the central design element, yielding a novel architecture in which structural knowledge becomes fixed once its stabilization is achieved.

Efficiency gains in DL have been pursued through both partial training and parameter-efficient adaptation. Methods such as FreezeOut [20], progressive freezing [21], and greedy layer-wise strategies [22] show that computation can be reduced by freezing stable components of the backbone without sacrificing accuracy. In parallel, the transfer learning literature has introduced parameter-efficient techniques that add small modules while leaving most of the backbone

untouched, including adapters [23], low-rank updates (LoRA, 24), bias-only tuning (BITFIT, 25), and prompt-based methods [26, 27] in NLP, as well as Side-Tuning [28], Visual Prompt Tuning [29], and AdaptFormer [30] in vision. While these approaches are effective, they all intervene directly in the backbone by modifying or extending its architecture. In contrast, GLAI follows the same philosophy of exploiting early stabilization for efficiency, but does so exclusively at the head level, leaving the pretrained backbone intact and providing an orthogonal path to resource savings.

Several learning settings highlight that the head plays a decisive role, much like in standard fine-tuning. In self-supervised representation learning, the architecture of the head is central: SimCLR demonstrated that a projection head is essential for disentangling invariances [31], while BYOL [32] and SimSiam [33] relied on predictors to stabilize training and improve downstream utility. Similarly, in few-shot learning, lightweight episodic classifiers such as Matching Networks [34], Prototypical Networks [35], Relation Networks [36], and MAML [37] enable rapid adaptation to novel classes with very limited data. Although these approaches pursue goals distinct from efficiency, they converge on the idea that head design is decisive for generalization. GLAI builds directly on this insight, providing a structured replacement for conventional MLPs that preserves accuracy while accelerating training, thereby extending the benefits of careful head design beyond specialized regimes to standard transfer learning scenarios.

Finally, lightweight protocols such as linear probing [38, 39] and angular classifiers like ArcFace [40] illustrate that even simple heads can provide valuable insights into representation quality or improve class separability without modifying the backbone. These methods are computationally inexpensive and therefore serve as practical lower bounds in transfer learning pipelines, but they typically fall short of the accuracy attainable with a full MLP head. GLAI builds upon this perspective by offering a head that remains efficient while matching the validation scores of conventional MLPs, thus surpassing the limitations of purely lightweight alternatives.

3. Theoretical Framework

This section introduces the mathematical framework underlying the GLAI framework. We begin by formalizing the notions of structural and quantitative knowledge through the representation of activation paths, showing that any MLP with ReLU activations can be reformulated by separating these two

components. Building on this result, we define GLAI as an alternative model and demonstrate that every MLP can be equivalently represented in this form. This section also includes other theoretical analysis like criteria for identifying the appropriate moment to apply GLAI during training, a method to construct GLAI models with parameter counts comparable to the original MLP, and a pruning criterion for the estimator.

3.1. Structural and Quantitative Knowledge in MLPs

We begin by formally defining what we mean by *structural* and *quantitative* knowledge in the context of MLPs. To set the stage, let us first fix the notation for the activation function. Hereafter, denote the ReLU function by $\sigma : \mathbb{R} \rightarrow \mathbb{R}$, defined as $\sigma(z) = \max(0, z)$. For brevity, the same symbol σ will also denote the component-wise extension $\mathbb{R}^n \rightarrow \mathbb{R}^n$, where $\sigma(z)_i = \sigma(z_i)$ for all $i \in \{1, \dots, n\}$.

Although the definition of an MLP is standard, we include it here briefly in order to unify notation and provide a consistent basis for the concepts introduced in this section.

Definition 1. A **Multilayer Perceptron (MLP)** with ReLU activation and L hidden layers is a mapping $f : \mathbb{R}^{n_0} \rightarrow \mathbb{R}^{n_{L+1}}$ that can be expressed as a composition $f = g_L \circ g_{L-1} \circ \dots \circ g_1 \circ g_0$, where $g_0 : \mathbb{R}^{n_0} \rightarrow \mathbb{R}^{n_1}$ is an affine mapping given by $g_0(x) = W_0 \cdot x + b_0$ with $W_0 \in \mathbb{R}^{n_1 \times n_0}$ and $b_0 \in \mathbb{R}^{n_1}$, and $g_l : \mathbb{R}^{n_l} \rightarrow \mathbb{R}^{n_{l+1}}$ is described as $g_l(x) = W_l \cdot \sigma(x) + b_l$, where $W_l \in \mathbb{R}^{n_{l+1} \times n_l}$ and $b_l \in \mathbb{R}^{n_{l+1}}$ for $l \in \{1, \dots, L\}$. In other words, f can be expressed as a composition

$$\mathbb{R}^{n_0} \xrightarrow{W_0 \cdot x + b_0} \mathbb{R}^{n_1} \xrightarrow{\sigma} \mathbb{R}^{n_1} \xrightarrow{W_1 \cdot x + b_1} \mathbb{R}^{n_2} \rightarrow \dots \rightarrow \mathbb{R}^{n_L} \xrightarrow{\sigma} \mathbb{R}^{n_L} \xrightarrow{W_L \cdot x + b_L} \mathbb{R}^{n_{L+1}},$$

alternating between affine transformations and ReLU activations.

For convenience, we denote by $f_l : \mathbb{R}^{n_0} \rightarrow \mathbb{R}^{n_{l+1}}$ the mapping $f_l = g_l \circ g_{l-1} \circ \dots \circ g_0$ for $l \in \{0, \dots, L\}$ that provides the intermediate values along the hidden layers in the neural network, in such a way that $f_0 = g_0$ and $f_L = f$.

Remark 1. As is well-established, any affine transformation in the form of $x \mapsto W \cdot x + b$ can be regarded as a linear transformation by augmenting the dimensionality of both the input and output spaces with an additional unit, owing to the identity:

$$\begin{bmatrix} W & b \\ 0 & 1 \end{bmatrix} \cdot \begin{bmatrix} x \\ 1 \end{bmatrix} = \begin{bmatrix} W \cdot x + b \\ 1 \end{bmatrix}.$$

Therefore, it is permissible, without loss of generality, to assume that $b_l = 0$ for all $l \in \{0, \dots, L\}$. Consequently, this theoretical section exclusively considers MLPs devoid of bias parameters.

A pivotal definition in this mathematical framework is that of activation pattern, as it will form the basis for the subsequent construction.

Definition 2. For a fixed sample $x \in \mathbb{R}^{n_0}$, a neuron is said to be **active** if the value it outputs is positive, and **inactive** otherwise. The **activation pattern** of x is defined as a list of L vectors $(\text{act}_1(x), \dots, \text{act}_L(x))$, where each $\text{act}_l(x) \in \{0, 1\}^{n_l}$ contains n_l binary values, determined based on whether the n_l neurons of layer l are active or inactive for the sample x . Formally, since the outputs of the n_l neurons of layer l are given by the vector $f_{l-1}(x) \in \mathbb{R}^{n_l}$, it follows that

$$\text{act}_l(x) = \sigma' \circ f_{l-1}(x),$$

where $\sigma'(z)_i = 1$ if $z_i > 0$, and $\sigma'(z)_i = 0$ otherwise.

The activation patterns of an MLP capture its expressive capacity, and their evolution during training is central to the model's ability to adapt to the data. A key phenomenon in ReLU-based MLPs is that the network behaves linearly on the subset of inputs $x \in \mathbb{R}^{n_0}$ that share the same activation pattern, as formalized in the following result:

Proposition 1. *Let $A = (A_1, \dots, A_L)$ denote a predefined activation pattern, and define the diagonal matrix $D_l = \text{diag}(A_l)$ of size $n_l \times n_l$ where the diagonal elements are determined by the vector $A_l \in \{0, 1\}^{n_l}$. Then, for every $x \in \mathbb{R}^{n_0}$ with activation pattern A , it holds that*

$$f(x) = W_L \cdot D_L \cdot W_{L-1} \cdot D_{L-1} \cdot \dots \cdot W_1 \cdot D_1 \cdot W_0 \cdot x.$$

Proof. We will prove by induction that $f_l(x) = W_l \cdot D_l \cdot \dots \cdot W_1 \cdot D_1 \cdot W_0 \cdot x$ for all $l \in \{0, \dots, L\}$. Since $f_L = f$, the result follows by setting $l = L$. For $l = 0$, the result is trivial, as $f_0(x) = W_0 \cdot x$ by definition. On the other hand, if x has activation pattern A , then $\text{act}_l(x) = A_l$, implying that $\text{diag}(\text{act}_l(x)) = D_l$. Moreover, it naturally holds that $\sigma(z) = \text{diag}(\sigma'(z)) \cdot z$, and thus

$$\begin{aligned} f_{l+1}(x) &= g_{l+1} \circ f_l(x) = W_{l+1} \cdot \sigma(f_l(x)) = W_{l+1} \cdot \text{diag}(\sigma'(f_l(x))) \cdot f_l(x) = \\ &= W_{l+1} \cdot \text{diag}(\text{act}_{l+1}(x)) \cdot f_l(x) = W_{l+1} \cdot D_{l+1} \cdot f_l(x). \end{aligned}$$

Hence, the result follows. □

Remark 2. The fact established in the preceding proposition is clearly not a novelty, though it remains relatively underrepresented in the literature. Notably, Sudjianto et al. [19, Theorem 1] already states this property in a related context. We include it here both for completeness and because we regard it as a fundamental yet underexploited perspective: despite its simplicity, the piecewise-linear nature of ReLU-based networks rarely appears explicitly in modern treatments, even though it provides valuable insight for the developments that follow.

Consequently, every ReLU-based MLP is a piecewise-linear function, where linearity holds within each region defined by a fixed activation pattern. In other words, activation patterns define regions of linearity of the network as a mapping. Once these stabilize, it is essentially a large but fixed piecewise-linear system.

Given a specific activation pattern, one can observe different paths across active neurons through which information flows in the MLP. This phenomenon motivates the following definition:

Definition 3. A **path** π of the MLP f is a tuple $\pi = (\pi_0, \dots, \pi_{L+1})$, where $\pi_l \in \{1, \dots, n_l\}$ for all $l \in \{0, \dots, L+1\}$. The index π_0 specifies the input coordinate where the path starts, the indices π_1, \dots, π_L indicate the positions of the hidden neurons traversed along the path, and π_{L+1} denotes the output neuron where the path ends.

Consequently, one can visualize a path π as a polygonal line across the neural network. Furthermore, each connection along a path, linking a neuron in layer l to one in layer $l+1$, is associated with a weight, *i.e.*, an element of the matrix W_l that determines the contribution when moving from one layer to the next. This suggests introducing the following concept:

Definition 4. The **weight of a path** $\pi = (\pi_0, \dots, \pi_{L+1})$ is the product of all the weights traversed along the path. Formally, if $w_{u,v}^l$ denotes the (i, j) coordinate of the weight matrix W_l associated with f_l , then the weight of π is defined as

$$\omega_\pi = w_{\pi_1, \pi_0}^0 w_{\pi_2, \pi_1}^1 \dots w_{\pi_{L+1}, \pi_L}^L.$$

Next, the concepts of active and inactive path are presented for a specific sample $x \in \mathbb{R}^{n_0}$, along with a couple of functions related to this notion.

Definition 5. Let $\pi = (\pi_0, \dots, \pi_{L+1})$ be a path of the neural network f .

1. Given a sample $x \in \mathbb{R}^{n_0}$, π is said to be **active path for x** if all hidden neurons through which π passes are active. Formally, this occurs when $\text{act}_l(x)_{\pi_l} = 1$ for all $l \in \{1, \dots, L\}$.
2. Denote the **indicator function** of π as the function $\text{ind}_\pi : \mathbb{R}^{n_0} \rightarrow \{0, 1\}$ defined as $\text{ind}_\pi(x) = 1$ when π is active for the sample x , and $\text{ind}_\pi(x) = 0$ otherwise.
3. Define the **contribution function** of π as the function $c_\pi : \mathbb{R}^{n_0} \rightarrow \mathbb{R}$ obtained as $c_\pi(x) = \text{ind}_\pi(x) \cdot x_{\pi_0}$, where x_{π_0} is the coordinate of x from which π starts. In other terms, $c_\pi(x)$ returns the coordinate of x from which path π originates when the path is active, and returns 0 otherwise.

The definition of the contribution function may initially appear arbitrary, yet its role becomes clear once we recognize that a path influences the MLP solely through the coordinate from which it originates. This perspective is formalized in the following theorem, which shows that f can be expressed as a linear combination of the contribution functions of all paths, each weighted by its corresponding parameters.

Theorem 1. *Let f be a ReLU-based MLP, let c_1, c_2, \dots, c_P denote the contribution functions of the P paths of f terminating at neuron i in the last layer, with $i \in \{1, \dots, n_{L+1}\}$, and let $\omega_1, \dots, \omega_P$ represent their associated weights. Then,*

$$f(x)_i = \sum_{p=1}^P \omega_p c_p(x).$$

Proof. Let $x \in \mathbb{R}^{n_0}$ be a fixed sample. By Proposition 1, if one writes $D_l = \text{diag}(\text{act}_l(x))$ for $l \in \{0, \dots, L\}$, it then follows that

$$f(x) = W_L \cdot D_L \cdot W_{L-1} \cdot D_{L-1} \cdot \dots \cdot W_1 \cdot D_1 \cdot W_0 \cdot x.$$

Rewriting this product in terms of the components $w_{u,v}^l$ of the matrices W_l , for a fixed $i \in \{1, \dots, n_{L+1}\}$, yields that

$$\begin{aligned} f(x)_i &= \sum_{i_L=1}^{n_L} \dots \sum_{i_0=1}^{n_0} w_{i,i_L}^L \text{act}_k(x)_{i_L} w_{i_L,i_{L-1}}^{L-1} \text{act}_{L-1}(x)_{i_{L-1}} \dots w_{i_2,i_1}^1 \text{act}_1(x)_{i_1} w_{i_1,i_0}^0 x_{i_0} \\ &= \sum_{i_L=1}^{n_L} \dots \sum_{i_0=1}^{n_0} w_{i_1,i_0}^0 \dots w_{i_L,i_{L-1}}^{L-1} w_{i,i_L}^L \text{act}_1(x)_{i_1} \dots \text{act}_{L-1}(x)_{i_{L-1}} \text{act}_L(x)_{i_L} x_{i_0}. \end{aligned}$$

On the one hand, the product of weights corresponds to the weight of the path passing through the neurons in positions i_0, \dots, i_L, i , which is the path $(i_0, i_1, \dots, i_L, i)$. On the other hand, notice that the definition given for active path yields that the indicator function can be calculated as the product of the binary values

$$\text{ind}_{(i_0, i_1, \dots, i_L, i)}(x) = \text{act}_1(x)_{i_1} \cdot \text{act}_2(x)_{i_2} \cdot \dots \cdot \text{act}_L(x)_{i_L}.$$

Indeed, the product is 1 if and only if each neuron of the path is active for x , and 0 otherwise. Hence, the product of the activations with the input x_{i_0} corresponds to the contribution function of the same path. It then follows that

$$f(x)_i = \sum_{i_L=1}^{n_L} \dots \sum_{i_0=1}^{n_0} w_{(i_0, i_1, \dots, i_L, i)} c_{(i_0, i_1, \dots, i_L, i)}(x).$$

As this summation is carried out over all paths terminating at neuron i in the last layer, a relabeling of the paths yields the expression

$$f(x)_i = \sum_{p=1}^P w_p c_p(x),$$

establishing the theorem’s statement. \square

Remark 3. A related formulation to Theorem 1 appears in Meng et al. [18], whose Equation (1) also expresses the output of a ReLU-based MLP as a sum over active paths with effective weights. While their result provides an expression that is mathematically close to ours, its role in their work is limited to the analysis of optimization dynamics. In contrast, our contribution lies in leveraging this decomposition as the foundation of a new architectural paradigm which explicitly exploits the separation between structural and quantitative knowledge to accelerate training. Thus, although the algebraic resemblance may not be entirely novel, the theoretical perspective and its implications for model design introduced here are completely original.

This demonstrates that every MLP can be expressed as a linear combination of the contribution functions of its constituent paths, weighted by their associated path weights. Specifically, this formally illustrates that the knowledge held by an MLP can be divided into two distinct types:

- The **structural knowledge**, entirely determined by the paths forming the model (specifically, through the contribution functions $c_p(x)$ of each path); and

- The **quantitative knowledge**, determined by the weights ω_p associated to the paths of the MLP.

This conceptual separation is not merely of theoretical interest. As will be shown later in Section 3.6, the structural component of a trained DNN stabilizes early during training and can be preserved without loss in validation scores. Consequently, once an MLP has reached a sufficiently mature stage of structural knowledge, it can be reformulated according to Theorem 1, allowing the training to focus solely on the linear component associated with quantitative knowledge. The framework derived from this reformulation provides the foundation for the developments presented in the rest of this work.

3.2. The GLAI Framework

Building on the previous definitions and results, we now formally introduce the GLAI framework, presented here for the first time in the literature. This framework defines a novel paradigm in which models are decomposed into two complementary components, corresponding to the two forms of knowledge inherent to an MLP: structural and quantitative.

The key idea is to abstract the notion of path in an MLP by retaining only its contribution function and associated weight. As shown in Theorem 1, this information suffices to recover the full output of the network. Models within the GLAI framework can thus be interpreted as linear with respect to the contribution functions, while these functions themselves encode the nonlinear structure of the data. This separation ensures fast training while preserving expressive power, since contribution functions capture meaningful nonlinearities.

Definition 6. A **GLAI model** designed to infer features $y \in \mathbb{R}^m$ from samples $x \in \mathbb{R}^n$ is a mapping $\phi : \mathbb{R}^n \rightarrow \mathbb{R}^m$, where for each $i \in \{1, \dots, m\}$, the output coordinate $y_i = \phi(x)_i$ is determined by

- (1) contribution functions $c_p(x)$, for $p \in \{1, \dots, P_i\}$, which return a fixed coordinate of x within a defined piecewise linear region of the sample space, and 0 otherwise; and
- (2) associated weights $\omega_p \in \mathbb{R}$ for $p \in \{1, \dots, P_i\}$,

so that

$$\phi(x)_i = \sum_{p=1}^{P_i} \omega_p c_p(x).$$

Remark 4. In the GLAI framework, the concept of path is abstracted: instead of corresponding to a specific sequence of neurons in the network, a “path” is represented solely by a contribution function and its associated weight. This abstraction extends the notion of path beyond the strict architecture of MLPs. Moreover, the number of paths used to define each output coordinate need not be identical, unlike in conventional MLPs.

According to Theorem 1, every ReLU-based MLP can be exactly expressed as a GLAI model, which implies that the class of functions realized by MLPs is strictly contained within that of GLAI. Since each output coordinate of a GLAI model is built as a finite affine combination of contribution functions, and these are piecewise affine, the resulting mapping is always piecewise affine. Thus, the GLAI framework preserves the desirable property of piecewise linearity while extending expressiveness beyond traditional MLPs.

A distinctive advantage of the GLAI representation is the notion of **path virtualization**, which treats paths as independent entities. In standard MLPs, different paths may overlap through shared neurons, so a change in a single parameter $w_{u,v}^i$ affects all paths that traverse neuron v in layer i and neuron u in layer $i + 1$. By contrast, the GLAI framework assigns independent weights to each path, effectively decoupling their influence. This virtualization enhances model flexibility and, as shown in Section 4, expands representational capacity compared to conventional MLPs. Furthermore, once the structural knowledge of the network has been fixed, path virtualization provides a mechanism to mitigate accuracy loss during retraining, a property confirmed empirically in our experiments.

In this setting, each coordinate $\phi(x)_i$ of a GLAI model f can be naturally described as a two-stage process. The first stage, the **path selector**, is defined by a mapping $S_i : \mathbb{R}^n \rightarrow \mathbb{R}^{P_i}$ that assigns to each input $x \in \mathbb{R}^n$ a vector $S_i(x) = (c_1(x), \dots, c_{P_i}(x))$, where each component $c_p(x)$ represents the contribution of a path associated with the output coordinate i . The second stage, the **estimator**, is a linear mapping $L_i : \mathbb{R}^{P_i} \rightarrow \mathbb{R}$, given by $L_i(c_1, \dots, c_{P_i}) = \omega_1 c_1 + \dots + \omega_{P_i} c_{P_i}$. Together, these two stages yield the decomposition $f(x)_i = L_i \circ S_i(x)$: first, the active paths are identified through $S_i(x)$, and then their contributions are aggregated by L_i through a weighted linear combination.

For a compact expression of the full output, let $S(x) = (S_1(x), \dots, S_m(x))$ denote the concatenated vector of all path contributions, with $P_1 + \dots + P_m$ entries ordered by their corresponding output coordinates. If ω_p^i denotes the

weight associated with path p targeting coordinate i , $\tilde{\omega}^i$ denotes the row vector $[\omega_1^i, \omega_2^i, \dots, \omega_{P_i}^i]$ and Λ denotes the matrix

$$\begin{bmatrix} \tilde{\omega}^1 & & & \\ & \tilde{\omega}^2 & & \\ & & \ddots & \\ & & & \tilde{\omega}^m \end{bmatrix} \in \mathbb{R}^{m \times (P_1 + \dots + P_m)},$$

then $f(x) = \Lambda \cdot S(x)^T$. This formulation highlights the two-stage nature of GLAI models: an input $x \in \mathbb{R}^n$ first propagates through the path selector stage, which determines the active paths and constructs $S(x)$. In the second stage, the estimator, a structured linear operator with parameter matrix Λ , combines these contributions to produce the output, with each path linked exclusively to a single output neuron (see Figure 1).

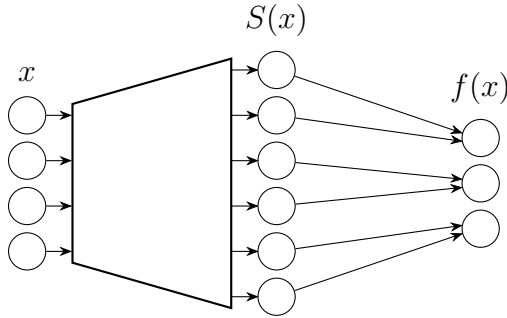


Figure 1: Representation of a GLAI model for samples $x \in \mathbb{R}^4$, target values $f(x) \in \mathbb{R}^3$. In this example representation, there are 6 paths in total, distributed in a ratio of 2 paths per output coordinate.

3.3. GLAI in Practice

In practical terms, applying GLAI requires starting from an MLP whose structural knowledge has reached a sufficiently stable stage. To establish a fair comparison and highlight the capabilities of GLAI, we begin with a reference MLP (hereafter the original MLP), chosen with an architecture suitable for the target task and trained until full convergence.

For the GLAI framework, however, we proceed differently. We start from a smaller MLP, trained only for a reduced number of epochs enough to ensure stabilization of its structural knowledge but not full convergence. At this

point, the GLAI framework is applied: the structural knowledge of the reduced network is frozen, and the model is rewritten as a linear estimator defined over the path space. Concretely, the estimator is a linear model with one parameter per path, operating on $S(x)$, which encodes for each input x the contribution functions of the corresponding paths. Although the number of paths grows exponentially with network depth, only a small fraction contributes effectively to the output. This redundancy enables aggressive pruning, drastically reducing the size of the estimator while preserving predictive accuracy.

The pruned estimator is then trained to convergence. The pruning ratio is selected so that the final estimator has a number of parameters equal to the difference between those of the original MLP and the reduced MLP, ensuring a fair comparison between MLP and GLAI. As a result, the full GLAI framework unfolds in two phases: (i) a short training stage for a reduced MLP, sufficient to stabilize structural knowledge, and (ii) the training of the pruned estimator obtained from rewriting this reduced MLP within the GLAI framework. Section 4 confirms that this two-phase procedure consistently requires substantially less training time than the original MLP, while achieving similar or even superior validation scores in most scenarios.

Figure 2 shows a diagram of how the GLAI pipeline is carried out in practice. First, the reduced MLP is trained and then stored as a fixed copy, which is used through forward passes to obtain the corresponding activations. Subsequently, the linear system derived from the estimator is trained by updating the weights associated with the paths, initialized from the already trained reduced model.

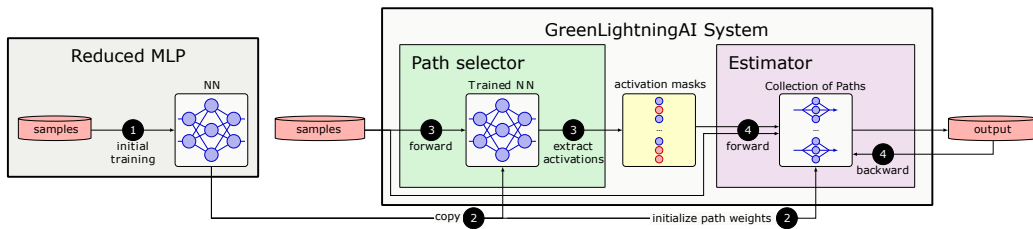


Figure 2: GLAI training process. A reduced MLP is first trained for a limited number of epochs to stabilize its structural knowledge. The network is then rewritten within the GLAI framework by splitting it into a fixed path selector, which preserves the learned structure, and a trainable linear estimator defined over the selected path contributions. Finally, the estimator is pruned and trained to convergence while the path selector remains frozen.

The next subsections present the implementation details on how the opera-

tions are performed as well as formalize the application criterion, the pruning strategy, and the parameter-count matching procedure used throughout our experiments.

3.4. Implementation

Listing 1 shows a simplified PyTorch implementation of the estimator. The computation first combines the input samples with the binary activations produced by the path selector, and then applies the estimator weights to obtain the output.

```

1 # x_input:      [batch_size, n_inputs]
2 # weight_act:  [batch_size, n_weights]
3 # self.weight: [n_outputs, n_inputs, n_weights]
4
5 outer = torch.einsum("bi,bs->bis",
6     (x_input, weight_act.float()))
7
8 output = torch.einsum("bis,ois->bo",
9     (outer, self.weight))

```

Listing 1: Reference PyTorch implementation of the path-conditioned estimator

Although this implementation is concise, it explicitly materializes the intermediate tensor containing the merged samples and path activations. To avoid this overhead, the optimized implementation uses custom CUDA kernels that directly accumulate the contribution of the active paths, as shown in Listing 2. The listing presents the computation as a sequential loop for clarity, while the actual CUDA kernel parallelizes the work across samples, outputs, and estimator components. As a result, the system only needs to store the weights and their gradients, together with the inputs and outputs of the DNN, in the same manner as any other DNN. A detailed comparison between the number of trainable parameters in GLAI and in an equivalent MLP is provided in Section 4.2.

```

1 for(o = 0; o < n_outputs; o++){
2     for(s = 0; s < n_samples; s++){
3         y[s,o] = 0;
4
5         for(i = 0; i < n_inputs; i++){
6             sum_weights = 0;
7
8             for(j = 0; j < n_weights; j++){
9                 sum_weights += weight_activations[s,j] * weights[i
10                ,j,o];
11             }
12             y[s,o] += sum_weights * x[s,i];
13         }
14     }

```

15 }

Listing 2: Forward estimator

Since the custom CUDA operation is not visible to PyTorch’s `autograd` system, the backward pass is implemented explicitly. Listing 3 shows the corresponding gradient computation for the estimator weights.

```

1 for(o = 0; o < n_outputs; o++){
2   for(s = 0; s < n_samples; s++){
3     dy_partial = dy[s,o];
4
5     for(i = 0; i < n_inputs; i++){
6       partial = x[s,i] * dy_partial;
7
8       for(j = 0; j < n_weights; j++){
9         dw[i,j,o] += weight_activations[s,j] * partial;
10      }
11    }
12  }
13 }
```

Listing 3: Backward estimator

The custom kernels therefore preserve the behavior of the reference implementation while avoiding the explicit construction of the intermediate path-conditioned tensor.

3.5. Path Distance Definition

We next introduce a notion of distance between two paths of a GLAI model. This definition will be a key ingredient in the remainder of this section, enabling the practical criteria and algorithms required to deploy GLAI.

To define the path distance function for a GLAI model $\phi : \mathbb{R}^{n_0} \rightarrow \mathbb{R}^{n_{L+1}}$, we fix a reference set $\Omega \subseteq \mathbb{R}^{n_0}$ on which ϕ is expected to achieve reliable scores. In practice, Ω can be chosen as the training or validation set, although the theoretical development remains valid for any arbitrary set Ω , whether finite or infinite.

Definition 7. Let Ω be a finite set, and consider two paths $\pi, \tilde{\pi}$ of ϕ originating from the same input coordinate x_i , with $i \in \{1, \dots, n_0\}$. The distance between π and $\tilde{\pi}$ with respect to Ω is defined as

$$d_{\Omega}(\pi, \tilde{\pi}) = \frac{1}{|\Omega|} \sum \{|x_i| : x \in \Omega, \text{ind}_{\pi}(x) \neq \text{ind}_{\tilde{\pi}}(x)\}.$$

Intuitively, $d_{\Omega}(\pi, \tilde{\pi})$ measures the number of samples $x \in \Omega$ for which the two paths are not simultaneously active or inactive, weighted by the magnitude of the initial input coordinate $|x_i|$, and normalized by the cardinality $|\Omega|$.

At a theoretical level, this definition can be extended to any set Ω equipped with a measure m . In that case, we define

$$d_{\Omega}(\pi, \tilde{\pi}) = \frac{1}{m(\Omega)} \int_{\{x \in \Omega: \text{ind}_{\pi}(x) \neq \text{ind}_{\tilde{\pi}}(x)\}} |x_i| dx.$$

Naturally, if Ω is finite and m is the counting measure, this integral reduces to the discrete definition above. For this reason, the theoretical exposition will employ the general measure-based notation, while keeping in mind that in practice Ω will typically be a finite subset of the training samples of the network. From now on, we will simply write $d(\pi, \tilde{\pi})$ whenever the reference set Ω is clear from context.

The next result reformulates the distance function in terms of the contribution functions:

Proposition 2. *Let c and \tilde{c} be the contribution functions associated with paths π and $\tilde{\pi}$, respectively. Then,*

$$d(\pi, \tilde{\pi}) = \frac{1}{m(\Omega)} \int_{\Omega} |c(x) - \tilde{c}(x)| dx.$$

Proof. Observe that $|\text{ind}_{\pi}(x) - \text{ind}_{\tilde{\pi}}(x)| = 1$ if and only if the paths π and $\tilde{\pi}$ are not simultaneously active or inactive for x . Since $c(x) = x_i \cdot \text{ind}_{\pi}(x)$ and $\tilde{c}(x) = x_i \cdot \text{ind}_{\tilde{\pi}}(x)$, it follows that

$$\int_{\{x \in \Omega: \text{ind}_{\pi}(x) \neq \text{ind}_{\tilde{\pi}}(x)\}} |x_i| dx = \int_{\Omega} |x_i| \cdot |\text{ind}_{\pi}(x) - \text{ind}_{\tilde{\pi}}(x)| dx = \int_{\Omega} |c(x) - \tilde{c}(x)| dx,$$

which completes the proof. \square

Recall that the normalized ℓ_1 -norm of an integrable function g over a set Ω is defined as

$$\|g\|_1 = \frac{1}{m(\Omega)} \int_{\Omega} |g(x)| dx.$$

This quantity corresponds to the average absolute value of g over Ω . With this notation, the formula from the previous proposition can be compactly expressed as

$$d(\pi, \tilde{\pi}) = \|c - \tilde{c}\|_1.$$

In other words, the distance between two paths can be interpreted simply as the ℓ_1 distance between their respective contribution functions.

In these terms, the set of paths can itself be regarded as a normed space, by identifying each path p originating from the coordinate x_r with its contribution function c . Specifically, we define

$$\|\pi\|_1 = \|c\|_1 = \frac{1}{m(\Omega)} \int_{\Omega} |c(x)| dx = \frac{1}{m(\Omega)} \int_{\{x \in \Omega: \text{ind}_{\pi}(x)=1\}} |x_i| dx.$$

This norm will be particularly relevant when deciding which paths to prune from an estimator that is too large, since many paths in the network exhibit sufficiently small norms to be safely disregarded.

3.6. GLAI Application Criterion Based on Path Distance

One of the first practical questions that arises when applying the GLAI framework is how many epochs are required before the structural knowledge of an MLP becomes sufficiently mature to justify replacing it with an equivalent GLAI model and retraining only its quantitative component. As previously discussed, Duato et al. [14] demonstrated that structural knowledge converges faster than the general knowledge of the MLP. However, determining the precise point of convergence remains an open challenge.

To address this, one can adapt the metric proposed in the cited work: activation patterns are computed for a set of samples at each epoch, and the distance between successive patterns for the same sample is averaged across the dataset. While this metric performs reasonably well in practice, the natural theoretical step after establishing the framework introduced here is to quantify differences in structural knowledge directly through paths, following an analogous procedure.

Formally, let Ω be a subset of training samples. After each epoch of standard training of an MLP, we compute the norms of the P paths of the network. Suppose training proceeds for T epochs, and denote by c_1^t, \dots, c_P^t the contribution functions at epoch $t \in \{1, 2, \dots, T\}$, which evolve as the network weights change (while the paths themselves remain fixed, their activations vary). We then define the metric

$$m_t = \frac{1}{P} \sum_{p=1}^P d(c_p^t, c_p^{t+1}),$$

which quantifies the change in structural knowledge of the MLP across consecutive epochs.

Figure 3 illustrates the behavior of the proposed metric throughout training. The right y -axes report both the path distance m_t and the distance between model weights, computed as the mean absolute difference of consecutive parameter values. The left y -axis displays the network’s validation loss, while the x -axis corresponds to training epochs. Training was carried out with a constant learning rate of 10^{-3} and weight decay of 10^{-2} using Stochastic Gradient Descent (SGD). Although more advanced optimizers or schedulers could have been employed, we deliberately opted for this simple setting to provide clean results, free from potential confounding effects due to dynamic hyperparameter updates. The comparison highlights the faster stabilization of path distances relative to model weights.

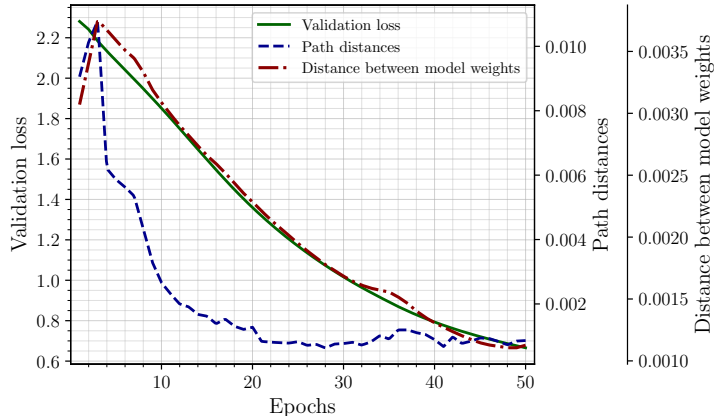


Figure 3: Evolution of the path distance m_t during training. The right y -axis corresponds to the relative error of m_t , while the left y -axis shows training and validation losses.

These results confirm, within the framework of this novel path-based metric, the earlier observations of Duato et al. [14]: structural knowledge stabilizes significantly earlier than the full convergence of the MLP, *suggesting it can be frozen at this stage while continuing to train only the quantitative knowledge*.

3.7. Estimator Pruning via Path Norms

Another practical issue that arises when applying the GLAI framework concerns the size of the estimator. When the layers of an MLP are compacted into a single layer, the number of paths grows exponentially with the depth of the network. Although this is not typically a severe limitation, since most

MLPs used in practice rarely exceed two hidden layers, it becomes important to control this growth in order to ensure a fair comparison between a standard MLP and its GLAI counterpart. This is achieved by pruning the paths of a GLAI model.

In practice, one may start with an MLP ϕ and consider an approximation $\tilde{\phi}$ with a reduced number of paths, under the expectation that this approximation remains sufficiently accurate so that the distance between ϕ and $\tilde{\phi}$ is small. To quantify the error between two GLAI models $\phi, \tilde{\phi} : \mathbb{R}^{n_0} \rightarrow \mathbb{R}$ with $n_{L+1} = 1$, over an arbitrary set Ω , we use

$$\|\phi - \tilde{\phi}\|_1 = \frac{1}{m(\Omega)} \int_{\Omega} |\phi(x) - \tilde{\phi}(x)| dx.$$

If Ω is finite (for instance, the training set in a practical scenario), $\Omega = \{x_1, \dots, x_m\}$, this reduces to

$$\|\phi - \tilde{\phi}\|_1 = \frac{1}{m} \sum_{k=1}^m |\phi(x_k) - \tilde{\phi}(x_k)|,$$

which corresponds to the average error across the samples x_k .

More generally, if $\phi, \tilde{\phi} : \mathbb{R}^{n_0} \rightarrow \mathbb{R}^{n_{L+1}}$, the distance can be computed by summing the distances between their coordinate functions $\phi_i, \tilde{\phi}_i : \mathbb{R}^{n_0} \rightarrow \mathbb{R}$ as

$$\|\phi - \tilde{\phi}\|_1 = \sum_{i=1}^{n_{L+1}} \|\phi_i - \tilde{\phi}_i\|_1.$$

The next result provides a practical criterion for compressing a GLAI model by reducing the number of active paths. As in the preceding sections, denote by $c_{1,i}, \dots, c_{P_i,i}$ the contribution functions of the P_i paths of ϕ associated to the neuron i of the last layer, with $i \in \{1, \dots, n_{L+1}\}$. Likewise, let $w_{1,i}, \dots, w_{P_i,i}$ be the associated weights, so that

$$\phi(x)_i = \sum_{p=1}^{P_i} w_{p,i} c_{p,i}(x)$$

for each $i \in \{1, \dots, n_{L+1}\}$.

Theorem 2. *Let $E \subseteq \{(p, i) \in \mathbb{N}^2 : 1 \leq p \leq P_i, 1 \leq i \leq n_{L+1}\}$ be the set of indices corresponding to the paths to be removed, where $(p, i) \in E$ if and only*

if the p -th path ending at neuron i is eliminated. Then the pruned network $\tilde{\phi}$ obtained by removing the paths in E satisfies that

$$\|\phi - \tilde{\phi}\|_1 \leq \sum_{(p,i) \in E} |w_{p,i}| \cdot \|c_{p,i}\|_1.$$

Proof. By the definition of E , let $E_i = \{p : (p, i) \in E\}$ be the set of indices of the paths removed that end at neuron i , with $i \in \{1, \dots, n_{L+1}\}$. Then

$$\phi(x)_i = \tilde{\phi}(x)_i + \sum_{p \in E_i} w_{p,i} c_{p,i}(x).$$

Hence,

$$\|\phi_i - \tilde{\phi}_i\|_1 = \left\| \sum_{p \in E_i} w_{p,i} c_{p,i}(x) \right\|_1 \leq \sum_{p \in E_i} |w_{p,i}| \cdot \|c_{p,i}\|_1.$$

Summing over all output coordinates gives

$$\|\phi - \tilde{\phi}\|_1 = \sum_{i=1}^{n_{L+1}} \|\phi_i - \tilde{\phi}_i\|_1 \leq \sum_{i=1}^{n_{L+1}} \sum_{p \in E_i} |w_{p,i}| \cdot \|c_{p,i}\|_1 = \sum_{(p,i) \in E} |w_{p,i}| \cdot \|c_{p,i}\|_1$$

as claimed. \square

Consequently, the set of paths can be pruned according to the values of the product between each path weight absolute value and its norm, namely the term $|w_{p,i}| \cdot \|c_{p,i}\|_1$ for the p -th path ending at neuron i . The error introduced by such pruning is in fact controlled, as it is bounded by the sum of these products over the discarded paths. To achieve a pruning factor $0 < \mu < 1$, meaning that only $100 \cdot \mu$ % of the paths are retained, one can compute the values $|w_{p,i}| \cdot \|c_{p,i}\|_1$ for all paths and select the top fraction corresponding to the desired quantile.

4. Experimental Results

The primary objective of this experimental section is to assess the practical value of the proposed GLAI framework, building upon the theoretical foundations introduced earlier. Rather than focusing solely on raw speed, our goal is to show that GLAI serves as an alternative to conventional fully connected heads in scenarios where such components are indispensable. In particular, we consider the widely adopted training paradigm where a lightweight head

is optimized on top of a frozen backbone, a setting that naturally highlights the efficiency and stability of the approach in practical scenarios.

To provide a broad evaluation, we design three families of experiments, each reflecting a different methodological context in which MLPs play a central role:

- (A) **Fixed embedding classification:** specializing pretrained models on downstream tasks beyond their original training domain.
- (B) **Self-supervision:** improving representation quality when abundant unlabeled data are available, using contrastive or predictor-style objectives.
- (C) **Few-shot learning:** adapting to entirely new tasks from only a handful of labeled examples.

These scenarios are of particular importance across diverse application domains, such as industrial inspection (A), autonomous driving (B), and medical imaging (C), among many others. Together, they demonstrate how GLAI can act as a drop-in replacement for MLPs while maintaining performance and reducing optimization burden.

Further technical details are provided in Subsection 4.1. Results are summarized in Subsection 4.3, and the parameter-budget matching procedure used to ensure a fair comparison is analyzed in Subsection 4.2.

4.1. Evaluation Details

This subsection provides additional technical details regarding the experimental setup used throughout Section 4. Within each family, we explore multiple configurations of backbones and datasets, systematically replacing conventional MLP heads with their GLAI-based counterparts. Concretely, Family A includes experiments (A1) DeiT-S/16 [10] on Oxford-IIIT Pets [41] and (A2) RoBERTa-base [42] on DBPedia-14 [43]. Family B covers (B1) EfficientNet-B0 [44] on STL-10 unsupervised split [45] and (B2) GPT-2 small [46] on WikiText-2 without labels [47]. Finally, Family C contains (C1) MobileNetV3-S [48] on Omniglot [49], and (C2) XLNet-base [50] on AGNews [43].

All the code used to conduct these experiments is available in the GitHub repository at <https://github.com/jmiravet/GLAI>.

The architectures in each experiment were chosen to represent different scales of the replaced models. We adopt the notation $(n_0, n_1, \dots, n_L, n_{L+1})$, where n_0 and n_{L+1} denote the number of input and output units respectively, and n_1, \dots, n_L the number of neurons in each of the L intermediate layers. The selected architectures are summarized in Table 1, where for each experiment (A1–C2) we list the corresponding tuple and the total parameter count (in millions).

Table 1: Architectures evaluated in the experiments.

Exp.	Backbone	Dataset	Arc. parameters	#Params (K)
A1	DeiT-S/16	Oxford Pets	(384, 256, 37)	108
A2	RoBERTa-base	DBPedia	(768, 128, 4)	100
B1	EfficientNet-B0	STL-10	(1280, 640, 128)	901
B2	GPT-2	WikiText-2	(768, 768, 128)	689
C1	MobileNetV3-Small	Omniglot	(576, 256, 5)	149
C2	XLNet-base	AGNews	(768, 512, 4)	396

The training procedure for GLAI consists of two phases. First, a conventional MLP is trained until convergence. Subsequently, an additional training stage is carried out for a reduced number of epochs to achieve structural convergence (see 3.6). This stage relies on a reduced-size MLP with reduction factor ρ (see 4.2), together with the corresponding μ associated with each ρ . The purpose of this step is to compress the estimator while preserving the alignment between structural and quantitative knowledge.

Regarding training setups, each family of experiments follows a dedicated protocol aligned with its intended objective. The **A-family** of experiments employs a standard supervised learning setup, where frozen backbones provide embeddings and trainable heads are optimized with cross-entropy loss for classification. This design mirrors classical fine-tuning pipelines commonly adopted in practice. The **B-family** focuses on unsupervised learning, where models act as projection heads trained with a contrastive loss. In this setting, dropout is applied only to the trainable projection layers (excluding the frozen backbone), in order to generate multiple stochastic views of the same input for the computation of the InfoNCE loss. The dropout rate is set to 0.2 in **B1** and 0.4 in **B2**, while the temperature parameter remains fixed at 0.07 in both cases. No data augmentation is employed, as the goal is to isolate the effect of the projection head and measure only the cost of its forward and

backward passes, avoiding additional computational overhead from repeated inferences through the backbone. Finally, the **C-family** targets few-shot learning. In **C1**, we adopt a 5-way 4-shot 6-query configuration, where each episode comprises 20 support images (4 per class) and 30 query images (6 per class). In **C2**, the setup extends to relation extraction with a 5-way 5-shot 10-query configuration, yielding 25 support sentences and 50 query sentences per episode. Both C-family experiments follow the meta-learning paradigm: support examples are used for adaptation within each episode, while query examples evaluate generalization to unseen samples of the same classes.

All conventional MLP baselines, including the reduced MLP, are optimized with SGD under the conditions reported in Table 2. For the GLAI estimator, we use Adam. This choice is motivated by the fact that, after the structural component has been fixed, GLAI no longer optimizes the same parameter space as a standard MLP: training is performed over path weights in a linear estimator defined on frozen path contributions. This induces a different optimization geometry, with gradients that can be more anisotropic and a loss landscape that is often flatter than in the original MLP parameterization. In this setting, using the same optimizer is not necessarily the fairest comparison, since SGD and adaptive methods interact differently with each parameterization. We therefore keep SGD for the conventional MLPs, where it provides a simple and stable baseline with minimal optimizer-induced effects, and use Adam for the GLAI estimator, where coordinate-wise adaptive updates provide more stable optimization. Importantly, the reported wall-clock times include the full cost of the optimizer used in each case, so the measured speedups correspond to the actual training pipelines being compared. A deeper study of optimizer behavior and loss-geometry in the GLAI parameter space is left for future work. Dropout was employed exclusively in the B-family experiments. The remaining hyperparameters are summarized in Table 2, including learning rate (LR) and batch size (BS), which are identical for both MLPs and GLAI. The table also reports the weight decay (WD) values, which differ between MLPs and their GLAI counterparts. This difference is intentional: WD was selected independently for each architecture so as to use the regularization setting that most benefits each model. In particular, after the replacement procedure, the GLAI estimator has a simpler, effectively single-layer structure, which makes it more prone to overfitting when weak regularization is used. For this reason, GLAI requires a stronger WD than the baseline MLP in order to improve generalization and provide a fair comparison between well-tuned versions of both approaches. Convergence

is determined by early stopping with identical parameter settings for each MLP and its corresponding GLAI, ensuring a fair comparison. Validation accuracy is monitored for the A- and C-families, whereas validation loss is monitored for the B-family. Patience and minimum delta parameters are set according to the experiment: patience of 5 and min delta of 0.1 for A1 and A2; patience of 5 and min delta of 10^{-5} for B1; patience of 5 and min delta of 0.01 for B2; and patience of 30 with min delta of 1 for the C-family.

For GLAI training, the values of WD and ρ (the reduction factor) are reported, along with the number of epochs dedicated to the reduced MLP stage (Red. Epochs in Table 2), which is chosen to guarantee structural convergence. Finally, the total number of epochs required for GLAI training is reported under Epochs to conv., representing the sum of the reduced MLP training epochs and the subsequent epochs until full convergence of the estimator.

Table 2: Training configurations and results. Experiments are identified by code only. Epochs to convergence are reported as mean \pm std across seeds.

Exp.	LR	BS	MLP Training		GLAI Training			
			WD	Epochs to conv.	WD	ρ	Red. epochs	Epochs to conv.
A1	0.001	16	0.001	60.00 ± 0.00	0.1	0.5	20	14.33 ± 3.21
A2	0.001	16	0.001	37.33 ± 3.06	0.1	0.5	20	6.67 ± 0.58
B1	0.001	16	0.001	31.33 ± 2.08	0.1	0.5	60	8.33 ± 3.51
B2	0.0001	16	0.01	9.33 ± 1.53	0.1	0.5	2	2.00 ± 0.00
C1	0.001	16	0.001	154.00 ± 110.69	0.1	0.5	30	43.67 ± 6.81
C2	0.001	32	0.01	78.00 ± 38.11	0.1	0.5	30	43.00 ± 7.81

Determining when the structural knowledge of an MLP has stabilized is a challenging problem, both theoretically and in practice, as it requires understanding the dynamics of activation patterns and designing reliable proxies to measure them. In this work, we adopt a simple and reproducible heuristic. For each experiment, we first estimate the number of epochs required for full convergence of the corresponding MLP, and then train the reduced MLP for a fixed fraction of this budget: 20% for Family A, 15% for Family B, and 10% for Family C. These values reflect the differences across training regimes and were found to provide a reasonable trade-off between structural maturity and efficiency. While this rule does not explicitly measure structural convergence, it offers a consistent practical criterion across all experiments.

All experiments were implemented in PyTorch and executed on a compute node running Ubuntu 18.04.5 LTS (Linux kernel 4.15.0). The node is equipped with two AMD EPYC 7282 processors (32 physical cores, 64 threads in total; 2 NUMA nodes; base frequency 1.5 GHz, maximum frequency 2.8 GHz) and ten NVIDIA A100 GPUs, each with 80 GB of memory. For all reported experiments, only a single A100 GPU was allocated and used. Jobs were submitted through Slurm with a memory request of 64 GB, although actual usage remained below this threshold.

4.2. Ensuring a Fair Comparison Between an MLP and Its GLAI Counterpart

Once the pruning procedure for reducing the number of paths in a GLAI model has been established, it is necessary to address how to guarantee a fair comparison between a conventional MLP and its associated GLAI model. This issue arises because the GLAI formulation requires the underlying MLP to perform the forward pass in order to compute the path activations, which are then weighted by the estimator.

Our investigation has shown that a straightforward yet effective strategy is to replace the original MLP with a smaller one, reduced by a fixed factor. Such a reduced MLP preserves the expressivity of activation patterns, can be trained more efficiently, and yields a GLAI model that outperforms the original MLP in training time while achieving comparable accuracy.

Formally, consider an original MLP with layer dimensions given by the tuple $(n_0, n_1, \dots, n_L, n_{L+1})$, where n_0 and n_{L+1} denote the input and output dimensions, respectively, and $L \geq 1$ is the number of hidden layers. We propose reducing each hidden layer size uniformly by a factor $0 < \rho < 1$, resulting in a reduced MLP with dimensions $(n_0, \rho \cdot n_1, \dots, \rho \cdot n_L, n_{L+1})$. To prevent a bottleneck² at the final hidden layer, we require $\rho \cdot n_L \geq n_{L+1}$.

The comparison proceeds as follows. The original MLP is trained to convergence. Its GLAI counterpart is obtained from the reduced MLP, which is trained for only a fraction of the epochs required by the original, a sufficient amount to ensure the convergence of structural knowledge as detailed in Subsection 3.6. At this point, the equivalent GLAI model is constructed from the reduced MLP and subsequently pruned by a factor μ to match its parameter count with that of the original MLP. Specifically, pruning ensures

²If $n_L = n_{L+1}$, the proposed method no longer applies and must be reconsidered. Since the experimental setups in this work do not involve architectures of this shape, we omit further discussion here.

that the sum of the parameters of the frozen reduced MLP (used only to compute activations) and the parameters of the estimator equals the number of parameters in the original model.

The pruning factor μ is determined analytically. Let the number of parameters of the original network be

$$O = \sum_{l=0}^L (n_l + 1) n_{l+1},$$

the number of parameters of the reduced network be

$$R = \rho \cdot \left(n_0 n_1 + n_L n_{L+1} + \sum_{l=0}^L n_{l+1} \right) + \rho^2 \cdot \sum_{l=1}^{L-1} n_l n_{l+1} + n_{L+1},$$

and the number of parameters of the estimator obtained from the reduced MLP be

$$E = \rho^d \cdot \prod_{l=0}^{L+1} n_l + \sum_{k=1}^{L+1} \rho^{L+1-k} \cdot \prod_{l=k}^{L+1} n_l.$$

Then, the pruning factor is given by $\mu = (O - R)/E$, which guarantees that the comparison between the original MLP and its GLAI counterpart is balanced.

Example 1. Consider experiment **B1**, where the original MLP has architecture (1280, 640, 128) and $O = 901\text{K}$ parameters. Using $\rho = 0.5$, the reduced MLP has $R = 225\text{K}$ parameters, while the complete estimator contains $E = 13\text{M}$ parameters before pruning.

To match the memory footprint of the original MLP, the estimator must keep $O - R = 901\text{K} - 225\text{K} = 676\text{K}$ parameters. Therefore, the required pruning factor is $\mu = (O - R)/E = 676\text{K}/13\text{M} \approx 5.2\%$. Thus, the final GLAI model combines the reduced MLP (225K parameters) with the pruned estimator (676K parameters), matching the 901K parameters of the original model.

Example 2. Consider a simple theoretical setting to illustrate a potential limitation of the method when applied to very deep MLPs. Although such architectures are uncommon in practice, analyzing this regime helps clarify the behavior in extreme cases.

Let us assume an MLP with depth d (i.e., d hidden layers) and a constant width of n neurons per layer. The total number of parameters in the original MLP is then $O = dn^2$. After applying a reduction factor ρ , the reduced

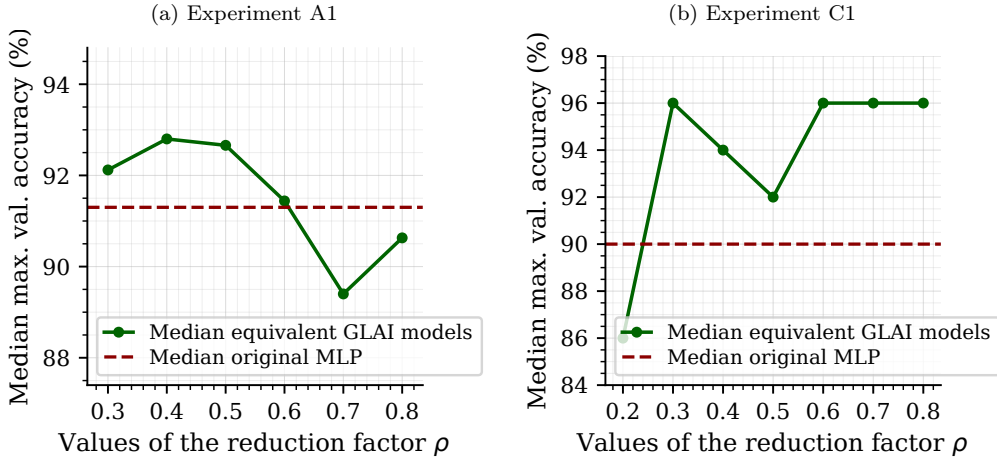


Figure 4: Maximum validation accuracy obtained by the original MLP and its GLAI counterparts for different reduction factors ρ .

model contains $R = d\rho n^2$ parameters, while the resulting estimator has size $E = \rho^{d+1}n^{d+1}$.

The key issue emerges from the exponential dependence of E on the depth d . As d increases, the estimator can grow rapidly, potentially leading to practical inefficiencies. In this setting, the corresponding pruning factor is given by

$$\mu = \frac{d(1 - \rho^2)}{\rho^{d+1}n^{d-1}}.$$

To provide a concrete illustration, consider $n = 128$, $d = 4$, and $\rho = 0.5$. In this case, we obtain $\mu \approx 4 \times 10^{-5}$, an extremely small value that may negatively affect the stability or effectiveness of the model.

While the estimator naturally enables aggressive pruning, this example highlights that, in certain edge cases, the required pruning levels may become excessively restrictive. This reinforces the importance of considering architectural depth when applying the method.

Remark 5. If ρ is too small, it may occur that $\mu > 1$. This means that the estimator contains fewer parameters than required to match the parameter count of the original MLP. In this case, one may either set $\mu = 1$ (i.e., avoid pruning and obtain a GLAI model with fewer parameters than the original) or select a larger value of ρ .

The balance between the two compression factors, ρ and μ , is delicate. While more sophisticated techniques for reducing the size of the MLP could be employed, the method described here has proven sufficient for the scale of the experiments considered. Since μ is determined as a function of ρ , the only remaining choice is the value of ρ . Figure 4 reports an ablation study on the effect of the reduction factor ρ in two representative settings: experiment A1 (Oxford-IIIT Pets + DeiT-S/16) and experiment C1 (Omniglot + MobileNetV3-S). The x -axis reports the value of ρ , while the y -axis shows the median validation accuracy obtained by the original MLP models and their corresponding GLAI counterparts.

The results show that the effect of ρ is not governed by a simple monotonic or low-order trend, reflecting the complexity of the transformations involved in replacing the original MLPs with GLAI modules. Nevertheless, the intermediate value $\rho = 0.5$ performs consistently well in both ablation settings. In particular, it remains robustly above the original MLP baseline and provides a stable choice across architectures and datasets. Based on this observation, we use $\rho = 0.5$ in the main experiments, as it represents a reasonable intermediate value that offers a consistent trade-off between reduction and validation performance.

4.3. Results

The experimental results are summarized in Table 3. For each configuration (A1–C2), the table reports four alternatives: the original MLP, a reduced MLP using the same reduction factor adopted by GLAI ($\rho = 0.5$), the corresponding GLAI model, and a linear head. All models are trained under the same Early Stopping criterion, so the reported number of epochs corresponds to training until convergence according to that criterion. Results are computed over three random seeds and reported as mean \pm standard deviation.

Since the task families use different validation objectives, the BVS (Best Validation Score) is the natural metric of each setting: maximum validation accuracy for the supervised and few-shot classification experiments in Families A and C, and minimum validation loss for the self-supervised experiments in Family B. A complementary comparison of the training cost is shown in

²Datasets in Family B are considered in their unlabeled form to match the unsupervised learning setting.

Table 3: Results across all experiment families (A: Fixed Embedding Classification; B: Self-Supervision³; C: Few-Shot Learning). Acronyms: *Exp.* denotes experiment; *Epochs* indicates the number of training epochs until early stopping, reported as mean \pm std across seeds; *Speedup* is the ratio of the early-stopped elapsed training time of the original MLP to that of each counterpart; and *BVS* stands for Best Validation Score (% for accuracy, dimensionless values for loss).

Exp.	Backbone / Dataset	Head	Epochs	Speedup	BVS
A1	DeiT-S/16 Oxford-IIIT Pets	MLP	60.00 \pm 0.00	1 \times	acc: 88.05 \pm 0.28 %
		MLP reduced	60.00 \pm 0.00	(1.01 \pm 0.02) \times	acc: 86.60 \pm 1.52 %
		GLAI	14.33 \pm 3.21	(2.54 \pm 0.52) \times	acc: 90.75 \pm 0.28 %
		Linear	53.00 \pm 7.55	(1.32 \pm 0.13) \times	acc: 90.57 \pm 0.21 %
A2	RoBERTa-base DBPedia-14	MLP	37.33 \pm 3.06	1 \times	acc: 97.70 \pm 0.01 %
		MLP reduced	37.00 \pm 1.00	(1.02 \pm 0.08) \times	acc: 97.68 \pm 0.03 %
		GLAI	6.67 \pm 0.58	(3.50 \pm 0.46) \times	acc: 97.89 \pm 0.16 %
		Linear	24.33 \pm 13.32	(2.68 \pm 2.16) \times	acc: 95.44 \pm 0.04 %
B1	EfficientNet-B0 STL-10	MLP	31.33 \pm 2.08	1 \times	loss: (1.63 \pm 0.55) $\cdot 10^{-4}$
		MLP reduced	23.33 \pm 2.89	(0.91 \pm 0.14) \times	loss: (1.87 \pm 0.25) $\cdot 10^{-4}$
		GLAI	8.33 \pm 3.51	(1.05 \pm 0.40) \times	loss: (1.70 \pm 0.53) $\cdot 10^{-4}$
		Linear	60.00 \pm 0.00	(0.81 \pm 0.05) \times	loss: (3.00 \pm 1.30) $\cdot 10^{-4}$
B2	GPT-2 small WikiText-2	MLP	9.33 \pm 1.53	1 \times	loss: 0.209 \pm 0.010
		MLP reduced	9.67 \pm 0.58	(0.97 \pm 0.12) \times	loss: 0.220 \pm 0.013
		GLAI	2.00 \pm 0.00	(1.56 \pm 0.25) \times	loss: 0.159 \pm 0.013
		Linear	6.33 \pm 1.15	(2.30 \pm 0.26) \times	loss: 0.181 \pm 0.002
C1	MobileNetV3-S Omniglot	MLP	154.00 \pm 110.69	1 \times	acc: 90.00 \pm 8.00 %
		MLP reduced	188.33 \pm 30.66	(0.91 \pm 0.64) \times	acc: 90.00 \pm 10.00 %
		GLAI	43.67 \pm 6.81	(1.85 \pm 1.24) \times	acc: 96.67 \pm 3.06 %
		Linear	198.33 \pm 25.42	(1.07 \pm 0.89) \times	acc: 95.33 \pm 6.43 %
C2	XLNet-base AGNews	MLP	78.00 \pm 38.11	1 \times	acc: 52.50 \pm 5.00 %
		MLP reduced	66.33 \pm 41.48	(2.43 \pm 2.69) \times	acc: 55.00 \pm 5.00 %
		GLAI	43.00 \pm 7.81	(0.92 \pm 0.48) \times	acc: 48.33 \pm 12.58 %
		Linear	74.67 \pm 22.14	(1.39 \pm 0.59) \times	acc: 51.67 \pm 3.82 %

Figure 5, which breaks down the normalized training time into reduced MLP training, conversion, and GLAI training stages relative to the original MLP.

A complementary comparison of the training cost is shown in Figure 5, which breaks down the normalized training time into reduced MLP training, conversion, and GLAI training stages relative to the original MLP.

The speedup column measures the ratio between the elapsed training time of the original MLP and that of each alternative. Therefore, values above 1 \times indicate faster training than the original MLP, whereas values below 1 \times indicate slower training. The Best Validation Score (BVS) reports the best validation accuracy for the supervised experiments in families A and C, and

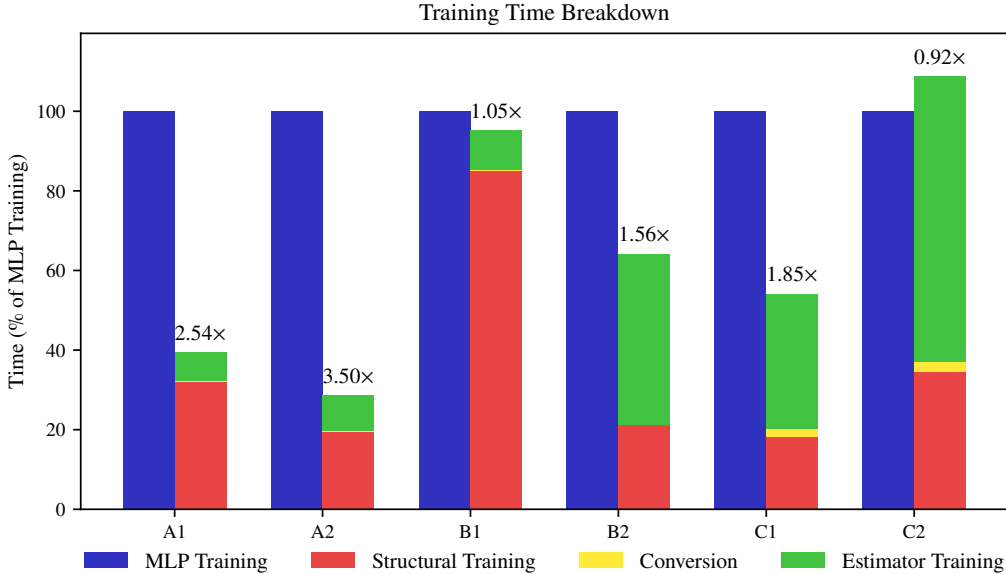


Figure 5: Normalized training time breakdown of GLAI relative to the baseline MLP. The stacked bars show the contributions of reduced MLP training, conversion, and GLAI training. Conversion time is negligible in some cases and may not be visible.

the minimum validation loss for the self-supervised experiments in family B.

In family A, GLAI provides a clear improvement in training efficiency while preserving, and even slightly improving, validation accuracy. In A1, GLAI reaches a speedup of $(2.54 \pm 0.52)\times$ over the original MLP, while obtaining a higher validation accuracy ($90.75 \pm 0.28\%$ versus $88.05 \pm 0.28\%$). A similar pattern is observed in A2, where GLAI achieves a speedup of $(3.50 \pm 0.46)\times$ and a validation accuracy of $97.89 \pm 0.16\%$, compared with $97.70 \pm 0.01\%$ for the original MLP. The relatively small deviations in these experiments indicate that the gains are consistent across seeds.

The behavior in family B depends on the specific self-supervised setting. In B1, GLAI and the original MLP show comparable training times, with a speedup of $(1.05 \pm 0.40)\times$. Their validation losses are also very close: $(1.70 \pm 0.53) \cdot 10^{-4}$ for GLAI and $(1.63 \pm 0.55) \cdot 10^{-4}$ for the original MLP. Given the magnitude of the standard deviations, these differences should be interpreted as practically negligible. Thus, in this setting, GLAI matches the original MLP rather than clearly outperforming it. In contrast, B2 shows a stronger advantage for GLAI: it obtains a lower validation loss (0.159 ± 0.013

versus 0.209 ± 0.010) together with a speedup of $(1.56 \pm 0.25)\times$, suggesting a more successful replacement in this configuration.

Family C exhibits higher variability, as expected in the few-shot learning setting, where the choice of seed can have a stronger effect on the final outcome. In C1, GLAI obtains a higher mean validation accuracy than the original MLP ($96.67 \pm 3.06\%$ versus $90.00 \pm 8.00\%$) and a speedup of $(1.85 \pm 1.24)\times$. Although this suggests a favorable trend for GLAI, the large standard deviations make the result less conclusive than in family A. In C2, GLAI reports a speedup of $(0.92 \pm 0.48)\times$, which nominally indicates slightly slower training than the original MLP; however, the high variability suggests that both methods have comparable training times in practice. The validation accuracies are also noisy in this setting, with GLAI obtaining $48.33 \pm 12.58\%$ compared with $52.50 \pm 5.00\%$ for the original MLP. Therefore, the few-shot experiments should be interpreted as cases where GLAI performs broadly on par with the original MLP, with trends that are informative but not as statistically stable as those observed in the fixed-embedding classification experiments.

As a final aggregate view, averaging the six per-experiment speedup ratios yields a mean speedup of $1.92\times$, so **GLAI trains at nearly twice the speed of the corresponding MLP on average**. This value is computed as the mean of ratios, not as the ratio of mean times. The dispersion is asymmetric, with deviations of $+1.25$ and -0.96 , indicating some variability across configurations but also a longer tail toward higher speedups. Overall, the aggregate timing results show a substantial reduction in training cost across the evaluated settings.

To complement the experiment-wise discussion, we further assess the results through paired hypothesis tests across all configurations. Since the experiments span heterogeneous domains, objectives, and score scales, we do not summarize the comparison through a raw average over BVS values. Instead, we construct paired contrasts over the (experiment, seed) pairs, yielding $n = 18$ paired observations: six experiments and three random seeds per experiment.

For training time, we define the oriented log-ratio

$$D_{\text{time}} = \log\left(\frac{T_{\text{MLP}}}{T_{\text{model}}}\right),$$

so that $D_{\text{time}} > 0$ indicates that the compared model converges faster than the original MLP. For validation performance, we define an oriented relative

Table 4: One-sided paired Wilcoxon tests against the original MLP, using $n = 18$ paired observations. For time, the alternative hypothesis is that the compared model converges faster than the original MLP. For BVS, the alternative hypothesis is that the compared model improves validation performance over the original MLP.

Comparison	Time p -value	BVS p -value
GLAI vs. MLP	0.0069	0.0276
Reduced MLP vs. MLP	0.4325	0.8597
Linear vs. MLP	0.0152	0.2475

score difference. For accuracy-based experiments,

$$D_{\text{score}} = \frac{S_{\text{model}} - S_{\text{MLP}}}{|S_{\text{MLP}}|},$$

whereas for loss-based experiments,

$$D_{\text{score}} = \frac{S_{\text{MLP}} - S_{\text{model}}}{|S_{\text{MLP}}|}.$$

Thus, in all cases, $D_{\text{score}} > 0$ indicates better validation performance than the original MLP. We then apply one-sided paired Wilcoxon signed-rank tests, where the null hypothesis corresponds to no positive paired advantage and the alternative hypothesis corresponds to faster convergence or better validation performance.

The results in Table 4 support the main hypothesis of the proposed method. The comparison between GLAI and the original MLP yields a low p -value for training time ($p = 0.0069$), providing statistical evidence that GLAI converges faster across the paired experiments. The BVS comparison also favors GLAI ($p = 0.0276$), although with a weaker margin than in the time comparison. This indicates that the speedup is not obtained at the expense of validation performance; rather, the paired evidence suggests that GLAI also improves the global validation score.

The two auxiliary baselines help qualify this result. The reduced MLP, which uses the same reduction factor as GLAI but without the proposed replacement mechanism, does not show evidence of either faster convergence ($p = 0.4325$) or improved validation performance ($p = 0.8597$). This suggests that the gains obtained by GLAI cannot be attributed merely to reducing the size of the original MLP. The linear model, in contrast, does show evidence

Table 5: One-sided paired Wilcoxon tests comparing GLAI against simplified alternatives, using $n = 18$ paired observations. The alternative hypothesis is that GLAI converges faster or obtains better validation performance than the corresponding baseline.

Comparison	Time p -value	BVS p -value
GLAI vs. Linear	0.0649	0.0564
GLAI vs. Reduced MLP	0.0038	0.0177

of faster convergence than the original MLP ($p = 0.0152$), which is expected given its simpler structure. However, it does not show evidence of improved validation performance ($p = 0.2475$). Therefore, while linear heads provide a strong efficiency baseline, they do not match the performance behavior observed for GLAI.

To further contextualize the role of these simplified alternatives, we also perform paired one-sided Wilcoxon tests directly comparing GLAI against the linear head and the reduced MLP. In these contrasts, the time statistic is defined as

$$D_{\text{time}} = \log \left(\frac{T_{\text{baseline}}}{T_{\text{GLAI}}} \right),$$

so that positive values indicate faster convergence for GLAI. The BVS statistic is analogously oriented so that positive values always indicate better validation performance for GLAI.

As shown in Table 5, GLAI is clearly favored over the reduced MLP in both training time ($p = 0.0038$) and validation performance ($p = 0.0177$). This reinforces the conclusion that the proposed mechanism provides benefits beyond a direct reduction of the MLP dimensionality. Against the linear model, the results are more nuanced. For the comparison against the linear model, the results are close to the conventional significance threshold in both dimensions: training time ($p = 0.0649$) and BVS ($p = 0.0564$). Although these values do not formally cross the 0.05 level, they consistently favor GLAI in both efficiency and validation performance. This is particularly relevant because the linear head constitutes a highly competitive efficiency-oriented baseline: it is expected to train quickly due to its reduced capacity, but this simplification does not provide the same validation behavior as GLAI. Therefore, the paired tests indicate that GLAI not only remains competitive with the linear alternative in terms of convergence time, but also tends to recover a stronger predictive profile across the heterogeneous experimental settings.

Overall, these paired tests provide a more robust summary than a direct average over heterogeneous experiments. GLAI is the only alternative that shows statistical evidence of both faster convergence and improved validation performance with respect to the original MLP. The reduced MLP does not reproduce these gains, and the linear model mainly captures the efficiency side without providing a reliable improvement in validation score. Taken together, the results support GLAI as an effective replacement for MLPs: it reduces the optimization burden while preserving, and in aggregate improving, validation performance across diverse experimental settings.

5. Conclusion

In this work we have introduced GLAI, a new architectural block that revisits the role of MLPs by separating structural from quantitative knowledge. Previous analyses [14] and our own theoretical and practical results (3.6) indicate that activation patterns stabilize significantly earlier than weights. We turn this observation into a training principle through the GLAI framework: once structural knowledge stabilizes, it is fixed, and training proceeds only on the quantitative component, which naturally collapses to a single-layer linear model.

Our experimental results show that this shift translates into consistent practical gains. GLAI models replace conventional MLP heads while maintaining accuracy, yet they require slightly less than 60% of the training time. Beyond speed, this reduction has tangible implications in terms of computational cost and energy use, thereby contributing to a more sustainable deployment of DL models.

Overall, GLAI emerges as an efficient alternative to conventional MLPs, grounded in both theoretical arguments and empirical evidence across diverse setups. By demonstrating that structural knowledge can be fixed early without loss of predictive power, this work opens the door to a broader line of research on path-based formulations. We expect that extending these ideas to more complex architectures may provide further insights into the interplay between expressivity, efficiency, and sustainability in modern DL.

6. Limitations and Future Work

The current implementation of GLAI is primarily intended for shallow MLP modules, such as the heads and projection layers evaluated in this

work. Its main practical limitation comes from the growth of the path space with depth: when the replaced MLP contains many hidden layers, the estimator may require very aggressive pruning, which can reduce stability or limit the potential efficiency gains. A second limitation concerns the particular reduction strategy adopted in this paper, which uniformly scales the hidden layers by a factor ρ and assumes $\rho \cdot n_L \geq n_{L+1}$ in order to avoid a bottleneck before the output layer. This constraint is not intrinsic to the GLAI formulation itself, but to the simple compression rule used here to construct the reduced MLP. If this condition is not satisfied in a given architecture, a different reduction or pruning strategy would be required. In many practical head and projection-layer settings, however, these conditions can be satisfied without difficulty, which is why the present formulation is sufficient for the scenarios studied in this work.

This study has focused on frozen-backbone scenarios, where the head is the main adaptation bottleneck. However, the architectural principle is not restricted to this setting. A major direction for future work is to investigate whether GLAI can be extended to large-scale architectures such as transformers. This extension is non-trivial: transformer models rely on tightly coupled attention, normalization, residual pathways, and feed-forward blocks, and replacing intermediate MLPs without disrupting these interactions requires careful theoretical and empirical analysis. Nevertheless, if these challenges can be addressed, such an extension could contribute to more efficient training and inference while also opening opportunities for interpretability in large-scale models. On the other hand, defining a reliable stopping criterion based on structural knowledge remains an open problem. Although it is known that activation patterns tend to stabilize earlier than weights, translating this behavior into a robust and task-independent proxy is still unresolved. Developing such a criterion, enabling early stopping driven by structural maturity rather than validation performance, is part of our ongoing work. Lastly, we are also exploring the use of synthetic weights and structural patterns to better characterize the interaction between structure and parameters.

Another relevant direction is to study how GLAI interacts with other efficiency-oriented techniques. The comparison in this work intentionally focuses on the vanilla MLP and vanilla GLAI formulations, in order to isolate the effect of the proposed architectural reformulation. However, GLAI is largely orthogonal to several acceleration, compression, and distillation strategies. In principle, methods such as distillation, improved training schedules,

specialized regularization, or further compression techniques could be applied on top of a GLAI module, just as they can be applied to conventional MLPs. Exploring these combinations is therefore a natural direction for future work.

Finally, a deeper understanding of the optimization geometry of GLAI remains necessary. The estimator does not optimize the same parameter space as a conventional MLP: after the structural component has been fixed, training takes place over path weights, leading to a different loss landscape. In our experiments, this change in parameterization also affects the behavior of regularization and optimizers, and suggests that the GLAI loss can be flatter in some regimes. This may make optimization less sensitive to some directions of descent and may explain why certain hyperparameter choices, such as stronger weight decay, are more beneficial for GLAI than for the original MLP. A systematic study of this parameter space, the geometry of the associated loss function, and the dynamics of different optimizers is left for future work.

Acknowledgments

This research was funded by the projects PID2023-146569NB-C21 and PID2023-146569NB-C22 supported by MICIU/AEI/10.13039/501100011033 and ERDF/UE. Jose I. Mestre was supported by the predoctoral grant ACIF/2021/281 of the *Generalitat Valenciana*. Alberto Fernández-Hernández was supported by the predoctoral grant PREP2023-001826 supported by MICIU/AEI/10.13039/501100011033 and ESF+. Cristian Pérez-Corral received support from the *Conselleria de Educació, Cultura, Universidades y Empleo* (reference CIACIF/2024/412) through the European Social Fund Plus 2021–2027 (FSE+) program of the *Comunitat Valenciana*. Manuel F. Dolz was supported by grant CNS2025-165098 funded by MICIU/AEI/10.13039/501100011033 and by the Plan Gen-T grant CIDEXG/2022/013 of the *Generalitat Valenciana*.

References

- [1] K. Hornik, M. Stinchcombe, H. White, Multilayer feedforward networks are universal approximators, *Neural Networks* 2 (1989) 359–366. doi:10.1016/0893-6080(89)90020-8.
- [2] G. Cybenko, Approximation by superpositions of a sigmoidal function, *Mathematics of Control, Signals and Systems* 2 (1989) 303–314. doi:10.1007/BF02551274.

- [3] K. Hornik, Approximation capabilities of multilayer feedforward networks, *Neural Networks* 4 (1991) 251–257. doi:10.1016/0893-6080(91)90009-T.
- [4] S. Hochreiter, J. Schmidhuber, Long short-term memory, *Neural Computation* 9 (1997) 1735–1780. doi:10.1162/neco.1997.9.8.1735.
- [5] Y. Lecun, L. Bottou, Y. Bengio, P. Haffner, Gradient-based learning applied to document recognition, volume 86, 1998, pp. 2278–2324. doi:10.1109/5.726791.
- [6] A. Krizhevsky, I. Sutskever, G. E. Hinton, Imagenet classification with deep convolutional neural networks, volume 60, Association for Computing Machinery, New York, NY, USA, 2017, p. 84–90. doi:10.1145/3065386.
- [7] A. Vaswani, N. Shazeer, N. Parmar, J. Uszkoreit, L. Jones, A. N. Gomez, L. Kaiser, I. Polosukhin, Attention is all you need, in: *Proceedings of the 31st International Conference on Neural Information Processing Systems, NIPS’17*, Curran Associates Inc., Red Hook, NY, USA, 2017, p. 6000–6010.
- [8] J. Devlin, M.-W. Chang, K. Lee, K. Toutanova, BERT: Pre-training of deep bidirectional transformers for language understanding, in: J. Burstein, C. Doran, T. Solorio (Eds.), *Proceedings of the 2019 Conference of the North American Chapter of the Association for Computational Linguistics: Human Language Technologies, Volume 1 (Long and Short Papers)*, Association for Computational Linguistics, Minneapolis, Minnesota, 2019, pp. 4171–4186. doi:10.18653/v1/N19-1423.
- [9] T. B. Brown, B. Mann, N. Ryder, M. Subbiah, J. Kaplan, P. Dhariwal, A. Neelakantan, P. Shyam, G. Sastry, A. Askell, S. Agarwal, A. Herbert-Voss, G. Krueger, T. Henighan, R. Child, A. Ramesh, D. M. Ziegler, J. Wu, C. Winter, C. Hesse, M. Chen, E. Sigler, M. Litwin, S. Gray, B. Chess, J. Clark, C. Berner, S. McCandlish, A. Radford, I. Sutskever, D. Amodei, Language models are few-shot learners, in: *Proceedings of the 34th International Conference on Neural Information Processing Systems, NIPS ’20*, Curran Associates Inc., Red Hook, NY, USA, 2020.

- [10] A. Dosovitskiy, L. Beyer, A. Kolesnikov, D. Weissenborn, X. Zhai, T. Unterthiner, M. Dehghani, M. Minderer, G. Heigold, S. Gelly, J. Uszkoreit, N. Houlsby, An image is worth 16x16 words: Transformers for image recognition at scale, 2021. [arXiv:2010.11929](https://arxiv.org/abs/2010.11929).
- [11] N. Shazeer, A. Mirhoseini, K. Maziarz, A. Davis, Q. Le, G. Hinton, J. Dean, Outrageously large neural networks: The sparsely-gated mixture-of-experts layer, 2017. [arXiv:1701.06538](https://arxiv.org/abs/1701.06538).
- [12] G. Montúfar, R. Pascanu, K. Cho, Y. Bengio, On the number of linear regions of deep neural networks, in: Proceedings of the 28th International Conference on Neural Information Processing Systems - Volume 2, NIPS'14, MIT Press, Cambridge, MA, USA, 2014, p. 2924–2932.
- [13] M. Raghu, B. Poole, J. Kleinberg, S. Ganguli, J. Sohl-Dickstein, On the expressive power of deep neural networks, in: D. Precup, Y. W. Teh (Eds.), Proceedings of the 34th International Conference on Machine Learning, volume 70 of *Proceedings of Machine Learning Research*, PMLR, 2017, pp. 2847–2854. URL: <https://proceedings.mlr.press/v70/raghu17a.html>.
- [14] J. Duato, J. I. Mestre, M. F. Dolz, E. S. Quintana-Ortí, J. Cano, Decoupling structural and quantitative knowledge in relu-based deep neural networks, in: Proceedings of the 5th Workshop on Machine Learning and Systems, EuroMLSys '25, ACM, New York, NY, USA, 2025, p. 39–45. doi:10.1145/3721146.3721950.
- [15] D. Hartmann, D. Franzen, S. Brodehl, Studying the evolution of neural activation patterns during training of feed-forward relu networks, *Frontiers in Artificial Intelligence Volume 4 - 2021* (2021). doi:10.3389/frai.2021.642374.
- [16] A. Fernández-Hernández, J. I. Mestre, M. F. Dolz, J. Duato, E. S. Quintana-Ortí, OUI need to talk about weight decay: A new perspective on overfitting detection, 2025. [arXiv:2504.17160](https://arxiv.org/abs/2504.17160).
- [17] B. Hanin, D. Rolnick, Complexity of linear regions in deep networks, in: K. Chaudhuri, R. Salakhutdinov (Eds.), Proceedings of the 36th International Conference on Machine Learning, volume 97 of *Proceedings*

- of *Machine Learning Research*, PMLR, 2019, pp. 2596–2604. URL: <https://proceedings.mlr.press/v97/hanin19a.html>.
- [18] Q. Meng, S. Zheng, H. Zhang, W. Chen, Z.-M. Ma, T.-Y. Liu, \mathcal{G} -sgd: Optimizing relu neural networks in its positively scale-invariant space, 2021. [arXiv:1802.03713](https://arxiv.org/abs/1802.03713).
- [19] A. Sudjianto, W. Knauth, R. Singh, Z. Yang, A. Zhang, Unwrapping the black box of deep relu networks: Interpretability, diagnostics, and simplification, 2020. [arXiv:2011.04041](https://arxiv.org/abs/2011.04041).
- [20] A. Brock, T. Lim, J. M. Ritchie, N. Weston, Freezeout: Accelerate training by progressively freezing layers, 2017. [arXiv:1706.04983](https://arxiv.org/abs/1706.04983).
- [21] G. Yuan, Y. Li, S. Li, Z. Kong, S. Tulyakov, X. Tang, Y. Wang, J. Ren, Layer freezing & data sieving: Missing pieces of a generic framework for sparse training, in: S. Koyejo, S. Mohamed, A. Agarwal, D. Belgrave, K. Cho, A. Oh (Eds.), *Advances in Neural Information Processing Systems*, volume 35, Curran Associates, Inc., 2022, pp. 19061–19074. URL: https://proceedings.neurips.cc/paper_files/paper/2022/file/794a425a2e47e05d29d30f79b79a692d-Paper-Conference.pdf.
- [22] E. Belilovsky, M. Eickenberg, E. Oyallon, Greedy layerwise learning can scale to ImageNet, in: K. Chaudhuri, R. Salakhutdinov (Eds.), *Proceedings of the 36th International Conference on Machine Learning*, volume 97 of *Proceedings of Machine Learning Research*, PMLR, 2019, pp. 583–593. URL: <https://proceedings.mlr.press/v97/belilovsky19a.html>.
- [23] N. Houlsby, A. Giurgiu, S. Jastrzebski, B. Morrone, Q. De Larousilhe, A. Gesmundo, M. Attariyan, S. Gelly, Parameter-efficient transfer learning for nlp, in: *Proceedings of the 36th International Conference on Machine Learning (ICML)*, volume 97 of *Proceedings of Machine Learning Research*, PMLR, 2019, pp. 2790–2799. URL: <http://proceedings.mlr.press/v97/houlsby19a.html>.
- [24] E. J. Hu, Y. Shen, P. Wallis, Z. Allen-Zhu, Y. Li, L. Wang, W. Chen, Lora: Low-rank adaptation of large language models, in: *Proceedings of the 10th International Conference on Learning Representations (ICLR)*, 2022. URL: <https://openreview.net/forum?id=nZeVKeeFYf9>.

- [25] E. Ben Zaken, Y. Goldberg, S. Ravfogel, Bitfit: Simple parameter-efficient fine-tuning for transformer-based masked language models, in: Proceedings of the 60th Annual Meeting of the Association for Computational Linguistics (ACL), 2022. URL: <https://aclanthology.org/2022.acl-short.1>.
- [26] B. Lester, R. Al-Rfou, N. Constant, The power of scale: Parameter-efficient adaptation for pretrained language models, in: Proceedings of the 2021 Conference on Empirical Methods in Natural Language Processing (EMNLP), Association for Computational Linguistics, 2021, pp. 3045–3059. URL: <https://aclanthology.org/2021.emnlp-main.243>.
- [27] X. L. Li, P. Liang, Prefix-tuning: Optimizing continuous prompts for generation, in: Proceedings of the 59th Annual Meeting of the Association for Computational Linguistics (ACL) and the 11th International Joint Conference on Natural Language Processing (IJCNLP), Association for Computational Linguistics, 2021, pp. 4582–4597. URL: <https://aclanthology.org/2021.acl-long.353>.
- [28] X. Zhang, Y. Chen, M. Yu, Y. Li, A. Yuille, S. Ullman, Side-tuning: A baseline for network adaptation via additive side networks, in: Computer Vision – ECCV 2020, volume 12347 of *Lecture Notes in Computer Science*, Springer, 2020, pp. 698–714. doi:10.1007/978-3-030-58580-8_41.
- [29] M. Jia, L. Tang, B.-C. Chen, C. Cardie, S. Belongie, B. Hariharan, S.-N. Lim, Visual prompt tuning, in: Computer Vision – ECCV 2022, volume 13664 of *Lecture Notes in Computer Science*, Springer, 2022, pp. 709–727. doi:10.1007/978-3-031-19827-4_41.
- [30] S. Chen, P. Zhuang, Q. Huang, X. Shen, L. Lin, Z. Li, Adaptformer: Adapting vision transformers for scalable visual recognition, in: Advances in Neural Information Processing Systems 35 (NeurIPS 2022), 2022. URL: <https://proceedings.neurips.cc/paper/2022/hash/fc0de4dcfe80b5e95bd8fda05bc6f8f3-Abstract-Conference.html>.
- [31] T. Chen, S. Kornblith, M. Norouzi, G. Hinton, A simple framework for contrastive learning of visual representations, in: Proceedings of the 37th International Conference on Machine Learning (ICML), volume 119 of *Proceedings of Machine Learning Research*, PMLR, 2020, pp. 1597–1607. URL: <http://proceedings.mlr.press/v119/chen20j.html>.

- [32] J.-B. Grill, F. Strub, F. Alché, C. Tallec, P. H. Richemond, E. Buchatskaya, C. Doersch, B. A. Avila Pires, Z. D. Guo, M. Gheshlaghi Azar, B. Piot, K. Kavukcuoglu, R. Munos, M. Valko, Bootstrap your own latent: A new approach to self-supervised learning, in: *Advances in Neural Information Processing Systems (NeurIPS)*, volume 33, 2020, pp. 21271–21284.
- [33] X. Chen, K. He, Exploring simple siamese representation learning, in: *Proceedings of the IEEE/CVF Conference on Computer Vision and Pattern Recognition (CVPR)*, 2021, pp. 15750–15758. doi:10.1109/CVPR46437.2021.01549.
- [34] O. Vinyals, C. Blundell, T. Lillicrap, K. Kavukcuoglu, D. Wierstra, Matching networks for one shot learning, in: *Advances in Neural Information Processing Systems (NeurIPS)*, volume 29, 2016.
- [35] J. Snell, K. Swersky, R. S. Zemel, Prototypical networks for few-shot learning, in: *Advances in Neural Information Processing Systems (NeurIPS)*, volume 30, 2017.
- [36] F. Sung, Y. Yang, L. Zhang, T. Xiang, P. H. S. Torr, T. M. Hospedales, Learning to compare: Relation network for few-shot learning, in: *Proceedings of the IEEE/CVF Conference on Computer Vision and Pattern Recognition (CVPR)*, 2018, pp. 1199–1208. doi:10.1109/CVPR.2018.00131.
- [37] C. Finn, P. Abbeel, S. Levine, Model-agnostic meta-learning for fast adaptation of deep networks, in: *Proceedings of the 34th International Conference on Machine Learning (ICML)*, volume 70 of *Proceedings of Machine Learning Research*, PMLR, 2017, pp. 1126–1135. URL: <http://proceedings.mlr.press/v70/finn17a.html>.
- [38] A. van den Oord, Y. Li, O. Vinyals, Representation learning with contrastive predictive coding, in: *Advances in Neural Information Processing Systems (NeurIPS) Workshop on Representation Learning*, 2018. arXiv:1807.03748.
- [39] M. Caron, H. Touvron, I. Misra, H. Jégou, J. Mairal, P. Bojanowski, A. Joulin, Emerging properties in self-supervised vision transformers,

- in: Proceedings of the IEEE/CVF International Conference on Computer Vision (ICCV), 2021, pp. 9630–9640. doi:10.1109/ICCV48922.2021.00951.
- [40] J. Deng, J. Guo, N. Xue, S. Zafeiriou, Arcface: Additive angular margin loss for deep face recognition, in: Proceedings of the IEEE/CVF Conference on Computer Vision and Pattern Recognition (CVPR), 2019, pp. 4690–4699. doi:10.1109/CVPR.2019.00482.
- [41] O. M. Parkhi, A. Vedaldi, A. Zisserman, C. V. Jawahar, Cats and dogs, in: 2012 IEEE Conference on Computer Vision and Pattern Recognition, 2012, pp. 3498–3505. doi:10.1109/CVPR.2012.6248092.
- [42] Y. Liu, M. Ott, N. Goyal, J. Du, M. Joshi, D. Chen, O. Levy, M. Lewis, L. Zettlemoyer, V. Stoyanov, RoBERTa: A Robustly Optimized BERT Pretraining Approach, Technical Report, Meta AI, 2019. arXiv:1907.11692.
- [43] X. Zhang, J. Zhao, Y. LeCun, Character-level convolutional networks for text classification, in: Advances in Neural Information Processing Systems, volume 28, 2015. arXiv:1509.01626.
- [44] M. Tan, Q. Le, EfficientNet: Rethinking model scaling for convolutional neural networks, in: K. Chaudhuri, R. Salakhutdinov (Eds.), Proceedings of the 36th International Conference on Machine Learning, volume 97 of *Proceedings of Machine Learning Research*, PMLR, 2019, pp. 6105–6114. URL: <https://proceedings.mlr.press/v97/tan19a.html>.
- [45] A. Coates, A. Ng, H. Lee, An analysis of single-layer networks in unsupervised feature learning, in: G. Gordon, D. Dunson, M. Dudík (Eds.), Proceedings of the Fourteenth International Conference on Artificial Intelligence and Statistics, volume 15 of *Proceedings of Machine Learning Research*, PMLR, Fort Lauderdale, FL, USA, 2011, pp. 215–223. URL: <https://proceedings.mlr.press/v15/coates11a.html>.
- [46] A. Radford, J. Wu, R. Child, D. Luan, D. Amodei, I. Sutskever, Language Models are Unsupervised Multitask Learners, Technical Report, OpenAI, 2019. URL: https://cdn.openai.com/better-language-models/language_models_are_unsupervised_multitask_learners.pdf.

- [47] S. Merity, C. Xiong, J. Bradbury, R. Socher, Pointer sentinel mixture models, 2016. [arXiv:1609.07843](https://arxiv.org/abs/1609.07843).
- [48] A. Howard, M. Sandler, B. Chen, W. Wang, L.-C. Chen, M. Tan, G. Chu, V. Vasudevan, Y. Zhu, R. Pang, H. Adam, Q. Le, Searching for mobilenetv3, in: 2019 IEEE/CVF International Conference on Computer Vision (ICCV), 2019, pp. 1314–1324. doi:10.1109/ICCV.2019.00140.
- [49] B. M. Lake, R. Salakhutdinov, J. B. Tenenbaum, Human-level concept learning through probabilistic program induction, *Science* 350 (2015) 1332–1338. doi:10.1126/science.aab3050.
- [50] Z. Yang, Z. Dai, Y. Yang, J. Carbonell, R. Salakhutdinov, Q. V. Le, Xlnet: Generalized autoregressive pretraining for language understanding, in: *Advances in Neural Information Processing Systems (NeurIPS)*, volume 32, 2019. URL: https://papers.nips.cc/paper_files/paper/2019/hash/dc6a7e655d7e5840e66733e9ee67cc69-Abstract.html.